



RR Lyrae Stars in the Newly Discovered Ultra-faint Dwarf Galaxy Centaurus I*

C. E. Martínez-Vázquez¹ , W. Cerny^{2,3} , A. K. Vivas¹ , A. Drlica-Wagner^{2,3,4} , A. B. Pace⁵ , J. D. Simon⁶ , R. R. Munoz⁷ , A. R. Walker¹ , S. Allam⁴ , D. L. Tucker⁴ , M. Adamów⁸ , J. L. Carlin⁹ , Y. Choi¹⁰ , P. S. Ferguson^{11,12} , A. P. Ji⁶ , N. Kuropatkin⁴ , T. S. Li^{6,13,21} , D. Martínez-Delgado¹⁴ , S. Mao^{15,16} , B. Mutlu-Pakdil^{2,3} , D. L. Nidever¹⁷ , A. H. Riley^{11,12} , J. D. Sakowska¹⁸ , D. J. Sand¹⁹ , and G. S. Stringfellow²⁰

(DELVE Collaboration)

¹ Cerro Tololo Inter-American Observatory, NSF's NOIRLab, Casilla 603, La Serena, Chile; clara.martinez@noirlab.edu

² Kavli Institute for Cosmological Physics, University of Chicago, Chicago, IL 60637, USA

³ Department of Astronomy and Astrophysics, University of Chicago, Chicago IL 60637, USA

⁴ Fermi National Accelerator Laboratory, P.O. Box 500, Batavia, IL 60510, USA

⁵ McWilliams Center for Cosmology, Carnegie Mellon University, 5000 Forbes Avenue, Pittsburgh, PA 15213, USA

⁶ Observatories of the Carnegie Institution for Science, 813 Santa Barbara Street, Pasadena, CA 91101, USA

⁷ Departamento de Astronomía, Universidad de Chile, Camino El Observatorio 1515, Las Condes, Santiago, Chile

⁸ Center for Astrophysical Surveys, National Center for Supercomputing Applications, 1205 West Clark Street, Urbana, IL 61801, USA

⁹ Rubin Observatory/AURA, 950 North Cherry Avenue, Tucson, AZ 85719, USA

¹⁰ Space Telescope Science Institute, 3700 San Martin Drive, Baltimore, MD 21218, USA

¹¹ George P. and Cynthia Woods Mitchell Institute for Fundamental Physics and Astronomy, Texas A&M University, College Station, TX 77843, USA

¹² Department of Physics and Astronomy, Texas A&M University, College Station, TX 77843, USA

¹³ Department of Astrophysical Sciences, Princeton University, Princeton, NJ 08544, USA

¹⁴ Instituto de Astrofísica de Andalucía, CSIC, E-18080 Granada, Spain

¹⁵ Department of Physics, Stanford University, 382 Via Pueblo Mall, Stanford, CA 94305, USA

¹⁶ Kavli Institute for Particle Astrophysics & Cosmology, P.O. Box 2450, Stanford University, Stanford, CA 94305, USA

¹⁷ Department of Physics, Montana State University, P.O. Box 173840, Bozeman, MT 59717-3840; NSF's National Optical-Infrared Astronomy Research Laboratory, 950 N. Cherry Avenue, Tucson, AZ 85719, USA

¹⁸ Department of Physics, University of Surrey, Guildford GU2 7XH, UK

¹⁹ Department of Astronomy/Steward Observatory, 933 North Cherry Avenue, Room N204, Tucson, AZ 85721-0065, USA

²⁰ Center for Astrophysics and Space Astronomy, University of Colorado, 389 UCB, Boulder, CO 80309-0389, USA

Received 2021 July 8; revised 2021 August 30; accepted 2021 August 31; published 2021 November 22

Abstract

We report the detection of three RR Lyrae (RRL) stars (two RRc and one R Rab) in the ultra-faint dwarf (UFD) galaxy Centaurus I (Cen I) and two Milky Way (MW) δ Scuti/SX Phoenicis stars based on multi-epoch *giz* DECam observations. The two RRc stars are located within two times the half-light radius (r_h) of Cen I, while the R Rab star (CenI-V3) is at $\sim 6 r_h$. The presence of three distant RRL stars clustered this tightly in space represents a 4.7σ excess relative to the smooth distribution of RRL in the Galactic halo. Using the newly detected RRL stars, we obtain a distance modulus to Cen I of $\mu_0 = 20.354 \pm 0.002$ mag ($\sigma = 0.03$ mag), a heliocentric distance of $D_\odot = 117.7 \pm 0.1$ kpc ($\sigma = 1.6$ kpc), with systematic errors of 0.07 mag and 4 kpc. The location of the Cen I RRL stars in the Bailey diagram is in agreement with other UFD galaxies (mainly Oosterhoff II). Finally, we study the relative rate of RRc+RRd (RRcd) stars (f_{cd}) in UFD and classical dwarf galaxies. The full sample of MW dwarf galaxies gives a mean of $f_{cd} = 0.28$. While several UFD galaxies, such as Cen I, present higher RRcd ratios, if we combine the RRL populations of all UFD galaxies, the RRcd ratio is similar to the one obtained for the classical dwarfs ($f_{cd} \sim 0.3$). Therefore, there is no evidence for a different fraction of RRcd stars in UFD and classical dwarf galaxies.

Unified Astronomy Thesaurus concepts: Pulsating variable stars (1307); Dwarf galaxies (416); Time domain astronomy (2109); RR Lyrae variable stars (1410); Local Group (929); Stellar astronomy (1583); Variable stars (1761)

Supporting material: machine-readable table

1. Introduction

The Λ cold dark matter cosmological model predicts that galaxies form hierarchically, with large galaxies formed by a continuous merging of low-mass systems (Searle & Zinn 1978; White & Frenk 1991; Frenk & White 2012). The dwarf satellite galaxies that we observe today may be the remnants of the merging process, and thus some authors refer to them as *surviving representatives of the halo's* building blocks (e.g., Fiorentino et al. 2015). The search for these building blocks has

provided the impetus for exceptional observational efforts targeting resolved Local Group dwarf systems (e.g., Tolstoy et al. 2009). However, the discovery of ultra-faint dwarf (UFD) galaxies located in the outer halo of our Galaxy has given a new perspective to the search for Galactic building blocks (Simon 2019, and references therein). These numerous (>40), old (>10 Gyr), and metal-poor ($[\text{Fe}/\text{H}] < -2$ dex) systems can have extremely low present-day luminosities ($L \sim 10^3\text{--}10^5 L_\odot$) and are considered to be among the most ancient relics of the formation of the Milky Way (MW; Bose et al. 2018).

Before the discovery of the first UFD galaxy a decade and a half ago (Willman et al. 2005a, 2005b), there was believed to be a clear distinction between dwarf galaxies and globular

* Based on DECam data.

²¹ NHFP Einstein Fellow.

clusters, since they were situated in different locations in the absolute V -band magnitude (M_V) versus physical half-light radius ($r_{1/2}$) plane (see, e.g., Figure 10 in Willman et al. 2005a). However, recently discovered systems with small sizes ($r_{1/2} \lesssim 80$ pc) and low luminosities ($M_V \gtrsim -6$ mag) cannot be definitively classified as star clusters or UFD galaxies without internal dynamics. Furthermore, the red giant branches (RGBs) of these systems are often so sparse, especially in shallow imaging, that their stellar populations and distances can only be determined at the most basic level. RR Lyrae (RRL) stars play an important role as unambiguous tracers of old stellar populations (>10 Gyr; Walker 1989; Savino et al. 2020) and standard candles (see, e.g., Beaton et al. 2018). They are pulsating variable stars with periods between ~ 7 hr and ~ 1 day and with typical amplitudes of several tenths of a magnitude (Smith 1995; Catelan & Smith 2015). RRL stars are excellent primary distance indicators due to their well-established optical/near-infrared period–luminosity relations (see, e.g., Cáceres & Catelan 2008; Marconi et al. 2015). Although the number of RRL stars in systems with $M_V > -3.5$ mag is expected to be of the order of 1 ± 1 stars (see Equation (4) in Martínez-Vázquez et al. 2019), the detection of even a single RRL star offers an independent and accurate distance to the host system (see, e.g., Vivas et al. 2016; Martínez-Vázquez et al. 2019). Improving the distance measurement to a system allows a better determination of the physical size and absolute magnitude, thus helping to determine its nature.

In addition, the period distribution of RRL stars provides clues about the contribution of the UFD galaxies to the formation of the MW halo (Stetson et al. 2014; Zinn et al. 2014; Fiorentino et al. 2015; Vivas et al. 2016; Fiorentino et al. 2017). While the inner halo has a period distribution peaked at $P \sim 0.55$ days, the outer halo has a period distribution shifted to longer periods. Increasing the observed population of RRL stars in UFDs will help us to ascertain how much of the long-period tail of field halo RRL stars can be attributed to disrupted UFDs.

Centaurus I (Cen I) is an ultra-faint system (absolute magnitude $M_V = -5.5$ mag, azimuthally averaged half-light radius $r_h = 2'.3$) discovered by Mau et al. (2020) in the DECam Local Volume Exploration survey (DELVE; Drlica-Wagner et al. 2021). DELVE combines archival DECam data with new observations to obtain complete coverage of the southern sky ($|b| > 10^\circ$). Data collection began in 2019A, with public DECam community data available through the NOIRLab Astro Data Archive.²² Cen I’s measured age ($\tau > 12.85$ Gyr), size ($r_{1/2} = 79_{-10}^{+14}$ pc), and systemic metallicity ($[\text{Fe}/\text{H}] = -1.8$ dex) place it within the size-magnitude locus consistent with most known UFDs (Mau et al. 2020). UFDs with similar brightness as Cen I have between 1 and 12 RRL stars (see Martínez-Vázquez et al. 2019; Vivas et al. 2020), and thus, we expect to detect several RRL in Cen I. In fact, using the N_{RRL} versus M_V relation from (Martínez-Vázquez et al. 2019, Equation (4)), Cen I is expected to contain 6 ± 2 RRL stars, which strongly motivates high-cadence observations of this system.

The paper is structured as follows. In Section 2 we present our observations and explain the details of the data reduction process. In Section 3, we describe the search method we used for detecting variable stars in the field of Cen I, and we report the variable stars detected in this work. In Section 4, we present the classification of the variable stars detected, their light

curves, and mean properties. We also show the color–magnitude diagram (CMD), the spatial distribution, and the proper motions (when available from Gaia) of stars in Cen I. In Section 5, we determine the distances of the RRL stars associated with Cen I. In Section 6, we perform the Oosterhoff classification (Oosterhoff 1939, 1944) of Cen I. In Section 7, we study the ratio of first overtone RRL stars in classical dwarf galaxies and UFDs. We investigate the angular size of Cen I in Section 8, and we conclude in Section 9.

2. Observations and Data

The data for this work were collected using the Dark Energy Camera (DECam; Flaugher et al. 2015) on the 4 m Blanco Telescope located at the NSF’s NOIRLab Cerro Tololo Inter-American Observatory (CTIO) in Chile. We obtained g , i , and z time-series photometry. The data were obtained in the second halves of 2020 February 8–10, 2020 March 4–7, and 2020 March 15–19 (PropID: 2020A-0238, P.I. Martínez-Vázquez). We observed two dithered fields, one centering Cen I on CCD N4 (one of the central DECam CCDs) and the other one dithering $60''$ in R.A. and $60''$ in decl. from the previous pointing in order to cover the gaps between CCDs. The majority of the data were obtained in gray nights; however, we also used bright nights of director’s discretionary time (where only z and i observations were made). The mean (median) seeing of the images is $1''.05$ ($1''.01$) in g , $0''.93$ ($0''.86$) in i , and $0''.91$ ($0''.87$) in z . In total, we collected 98 exposures: 35 g -band, 39 i -band, and 25 z -band exposures. Individual exposure times were 180 s in g and i , and 300 s in z , which allowed us to reach g , i , $z \sim 21$ mag with a signal-to-noise ratio $\gtrsim 50$ for single exposures.

We processed all exposures using the Dark Energy Survey (DES) Data Management (DESDM) pipeline (Morganson et al. 2018) following the procedure described in Drlica-Wagner et al. (2021). The DESDM pipeline achieves sub-percent-level photometric accuracy by calibrating exposures based on seasonally averaged bias and flat images and by performing full-exposure sky background subtraction (Bernstein et al. 2018). This pipeline utilizes SExtractor and PSFEX (Bertin & Arnouts 1996; Bertin 2011) for automatic source detection and photometric measurement on an exposure-level basis. Stellar positions are calibrated against Gaia (Gaia Collaboration et al. 2016) Data Release 2 (DR2; Gaia Collaboration et al. 2018), which provides 30 mas astrometric calibration precision. The photometry is calibrated by matching stars in each CCD to the Asteroid Terrestrial-impact Last Alert System (ATLAS) Refcat2 catalogs (Tonry et al. 2018), which consist of measurements from The Panoramic Survey Telescope & Rapid Response System DR1 (PS1; Chambers et al. 2016) and SkyMapper DR1 (Wolf et al. 2018) transformed to the PS1 griz filter system. For this calibration, stars were defined as objects passing a filter of $|\text{SPREAD_MODEL_}(BAND)| < 0.01$. Photometric measurements from the ATLAS Refcat2 catalog were transformed to the DECam giz filters before calibration using the following empirically derived equations:

$$\begin{aligned} g_{\text{DECam}} &= g_{\text{PS1}} + 0.0994(g_{\text{PS1}} - r_{\text{PS1}}) - 0.0319 \\ i_{\text{DECam}} &= i_{\text{PS1}} - 0.3407(i_{\text{PS1}} - z_{\text{PS1}}) - 0.0013 \\ z_{\text{DECam}} &= r_{\text{PS1}} - 0.2575(r_{\text{PS1}} - z_{\text{PS1}}) - 0.0201, \end{aligned}$$

which have statistical rms calibration errors per CCD estimated relative to DES of ~ 0.01 mag (see Drlica-Wagner et al. 2021).

²² <https://astroarchive.noao.edu/>

The typical photometric uncertainties for the horizontal-branch (HB) stars of Cen I are of the order of 0.005 mag.

In addition to our high-cadence observations, we also included individual *giz* DECam images previously processed by DELVE in the field of Cen I.²³ These exposures were processed identically through the same pipeline described above. Further information on the DELVE photometric pipeline can be found in Drlica-Wagner et al. (2021).

3. Search for Variable Stars

To search for variable stars, we first constructed a multiband source catalog by matching detections between individual exposures, following the procedure outlined in Drlica-Wagner et al. (2021). For this catalog only, we cross-matched all unique sources detected in the individual exposures with a $0''.7$ matching radius, and calculated weighted-average photometry for each source based on their measurements in each exposure and their associated uncertainties.

We calculated the extinction due to foreground dust from the MW for each individual source in the time-series and multiband catalogs through bilinear interpolation from the rescaled versions of the extinction maps of Schlegel et al. (1998) presented in Schlafly & Finkbeiner (2011). We then calculated the reddening for each source by assuming a reddening law of $R_V = 3.1$ and utilizing a set of coefficients $R_\lambda = A_\lambda / E(B - V)$ derived by the DES (DES Collaboration et al. 2018) for the *giz* bands.

We performed a search for periodic variable sources within $25'$ centered at the previously identified centroid for Cen I ($\alpha_{J2000} = 189^\circ 585$, $\delta_{J2000} = -40^\circ 902$) in the region of the CMD defined by $-0.5 \leq (g - i) \leq 0.6$ mag and $18.0 \leq g \leq 22.5$ mag. This region covers the instability strip of Cen I, where pulsating variable stars are located—specifically, RRL stars and Anomalous Cepheids (see, e.g., Sculptor, Martínez-Vázquez et al. 2016; or Sextans, Vivas et al. 2019). These selections produced hundreds of sources. As a variability index, we calculated a reduced chi-squared χ_ν^2 (see Sokolovsky et al. 2016) for each star by comparing a given star’s individual point-spread function measurements to the median magnitude of that same star across all epochs for the *g* band. Sources with $\chi_\nu^2 > 1$ were considered as potential variable candidates. We looked through all of the time series in the sources selected to check whether they showed a reliable variation in their light curves. We produced periodograms as a Fourier transform of the time-series data following the prescription described in Horne & Baliunas (1986). The periodograms were calculated between 0.01 and 10 days, in order to encompass all of the possible periods of RRL stars, Anomalous Cepheids, and possible short-period variables, such as δ Scuti (δ Sct) or SX Phoenicis (SX Phe) stars. Once periodicity was confirmed, we obtained the first estimation of the period from the highest peak in the periodograms, but the final period was refined by visually inspecting the folded light curves in the three bands simultaneously. In addition, we visually inspected all potential candidates in the images to remove spurious detections. The vast majority of spurious detections were background galaxies. Finally, we detected three RRL stars and two δ Sct/SX Phe stars in our sample.

²³ From 2013 March, and 2017 March–April.

4. Variable Stars in the Field of Cen I

The most common types of RRL stars are the *ab*-type (RRab) and *c*-type (RRc). RRab stars are fundamental pulsators characterized by longer periods (~ 0.45 – 1.0 days) and saw-tooth light curves while RRc stars are first overtone pulsators with shorter periods (~ 0.2 – 0.45 days), lower amplitudes ($\Delta V \simeq 0.4$ mag), and almost sinusoidal light variations. We detected three RRL stars (two RRc and one RRab) in the field of Cen I. Since our photometry reaches several magnitudes below the HB and the observing strategy (cadence) was meant to search for RRL stars, we expect $\sim 100\%$ completeness for detecting isolated RRL stars.²⁴

Assuming a smooth distribution of Galactic halo RRL stars (see, e.g., Zinn et al. 2014; Vivas et al. 2016), it is unlikely to find three RRL stars clumped together in space at large galactocentric distance. If we integrate the number density profile of RRL stars derived in Medina et al. (2018)—which is appropriate for the outer Galactic halo out to distances of ~ 150 kpc—we find that 0.15 RRL stars are expected in a search area of 0.54 sq. deg. in the range of distances between 40 and 245 kpc (i.e., covering the magnitude limits of our search). The probability of finding three or more Galactic halo RRL stars within this region is $p = 5 \times 10^{-4}$, which corresponds to a one-sided Gaussian significance of 3.3σ . In particular, if we estimate the number of MW halo RRL stars between 100 and 140 kpc that can contaminate our HB, the number is reduced to 0.02 RRL stars. The probability of finding three or more MW halo RRL stars in this case is $p = 1.3 \times 10^{-6}$, which corresponds to a one-sided Gaussian significance of 4.7σ . Thus, these three RRL stars are high confidence members of Cen I.

Additionally, we detected two δ Sct/SX Phe variables of the MW. They are classified as δ Sct/SX Phe stars because their periods are shorter than 0.1 day and their light curves are typical for this type of variable stars (see, e.g., Martínez-Vázquez et al. 2021). Furthermore, they are identified as MW field stars and not as members of Cen I because they are pulsating main-sequence stars (δ Sct) or blue straggler stars (SX Phe) and are thus significantly closer than Cen I (see Catelan & Smith 2015).

Figure 1 shows the light curves in the different filters and Table 1 provides the individual epoch photometry for all of these variable stars. It is worth noting that the light curve of Cen I-V3 has half the number of epochs (since it fell in one of the gaps between the DECam CCDs) and its phase space is not fully covered, particularly reflected as a lack of maximum in the light curve (see third top panel in Figure 1). We derive the pulsation parameters for the variable stars, obtaining the intensity-averaged magnitudes and amplitudes by fitting the light curves with the set of templates based on Layden (1998). The mean magnitudes were calculated using the best-fitting template, thus preventing biases in case light curves are not uniformly sampled in phase. Table 2 lists the coordinates and the pulsation parameters of the variable stars detected in the vicinity of Cen I.

Figure 2 displays the CMD of the stars found in the central $7'$ radius (gray points) of Cen I, the candidate members of Cen I according to Mau et al. (2020; i.e., $p_{\text{ugali}} > 0.05$, red points),²⁵

²⁴ We note that a variable source located within $0''.7$ of another source would be harder to recover due to the angular cross-matching that is performed to associate sources across individual exposures (see Section 3).

²⁵ This membership is based on the spatial position, measured flux, photometric uncertainty, and the local imaging depth, with an initial mass function weighting. It was obtained from the ultra-faint galaxy likelihood toolkit, *ugali*: <https://github.com/DarkEnergySurvey/ugali> (Bechtol et al. 2015; Drlica-Wagner et al. 2015).

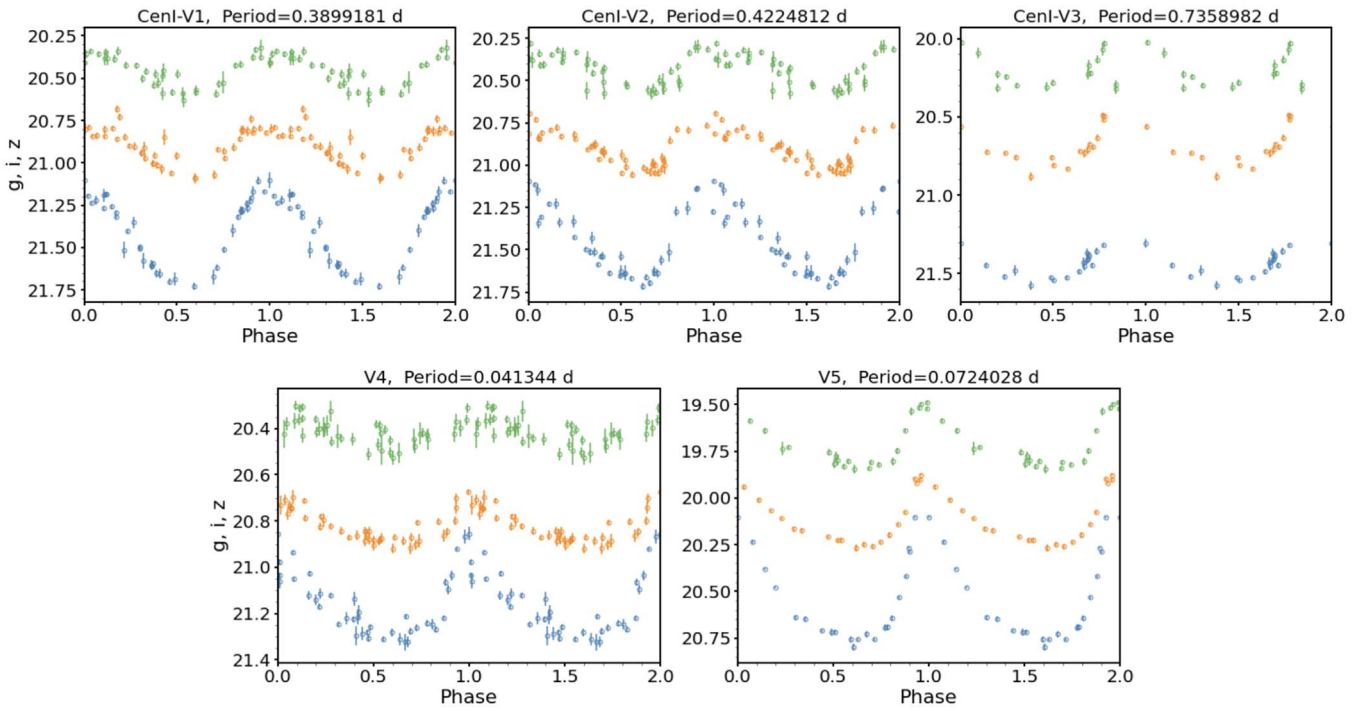


Figure 1. Light curves of the variable stars detected in the field of Cen I in the g (blue), i (orange), and z (green) bands, phased with the period in days given at the top of each panel. The name of the variable is also displayed. For clarity, the g and z light curves have been shifted to $+0.2$ and -0.4 mag, respectively. RRL stars of Cen I are displayed in the top panels while the field δ Sct/SX Phe stars are in the bottom panels.

Table 1
Photometry of the Variable Stars Found in the Field of Cen I

MJD_g	g	σ_g	MJD_i	i	σ_i	MJD_z	z	σ_z
CenI-V1								
56373.2754	20.987	0.014	56357.1475	20.933	0.021	56357.1449	20.925	0.065
56373.2768	20.984	0.015	57831.0747	20.808	0.028	56360.1379	20.885	0.039
57831.0729	21.085	0.025	57831.0875	20.815	0.028	56360.1389	20.852	0.038
57831.0738	21.087	0.025	58888.2045	20.800	0.027	56361.1419	20.809	0.031
57831.0858	21.045	0.025	58888.2451	20.803	0.024	56361.1430	20.807	0.031
57831.0866	21.067	0.026	58888.2874	20.849	0.021	56373.2729	20.784	0.040
58888.2020	20.903	0.047	58888.3292	20.972	0.024	56373.2792	20.783	0.042
58888.2426	20.992	0.039	58889.2138	21.092	0.030	57849.0516	20.719	0.045
58888.2850	21.315	0.050	58889.2555	21.070	0.026	57850.0564	20.990	0.035
58888.3268	21.378	0.047	58889.2961	20.908	0.022	57850.0581	21.029	0.044
...

Note. MJD is the Modified Julian Date of mid-exposure.

(This table is available in its entirety in machine-readable form.)

and the variable stars found in this work. The three RRL stars (blue stars) are well positioned over the HB, while the two variables brighter than the HB (orange crosses) have periods shorter than 0.08 days and are field δ Sct/SX Phe foreground stars.

Figure 3 shows the spatial distribution of the variable stars in the sky. Two of the RRL stars are within $2 r_h$ (specifically between 1 and $2 r_h$) while the third RRL is at $\sim 6 r_h$. An examination of whether the latter is an extra-tidal member of Cen I is presented Section 8.

4.1. Cross-matching with Gaia DR2 and Gaia EDR3

Within a radius of $25'$ (i.e., $\sim 10 r_h$) from the center of Cen I, Gaia DR2 (Gaia Collaboration et al. 2018; Holl et al. 2018)

flags only one star as “VARIABLE,” but no pulsation parameters nor proper motions are given for this star. When matching with our catalog, this star turned out to be V4, a δ Sct/SX Phe from the MW field. The mean value of G for this star is 20.14 mag, which is consistent with the mean g magnitude we obtain.

Using Gaia Early Data Release 3 (EDR3; Gaia Collaboration et al. 2021), we find proper motions for three of our variable stars, the two δ Sct/SX Phe stars (V4 and V5), and one of the Cen I RRL stars (CenI-V2). The remaining two Cen I RRL are either not in the catalog (CenI-V3) or do not have an astrometric solution (CenI-V1). Table 3 lists the Gaia EDR3 source\inferior id and proper motions for these stars.

In Figure 4, we compare the proper motion for CenI-V2 and the two δ Sct/SX Phe stars with candidate RGB members of

Table 2
Coordinates, Pulsation Properties, and Average Photometry of the Variable Stars in Cen I

Star	R.A. (degrees)	Decl. (degrees)	r^a (arcmin)	Period (days)	g (mag)	i (mag)	z (mag)	Δg^b (mag)	Δi^b (mag)	Δz^b (mag)	Type
CenI-V1	189.570323	-40.939879	2.38	0.3899181	21.24	20.92	20.86	0.56	0.25	0.24	RRc
CenI-V2	189.633635	-40.878072	3.37	0.4224812	21.20	20.88	20.83	0.53	0.27	0.20	RRc
CenI-V3	189.584351	-41.101214	13.12	0.7358982	21.21	20.67	20.59	>0.27	>0.36	>0.26	RRab
V4	189.516808	-40.744898	12.86	0.0413440	20.96	20.82	20.81	0.37	0.19	0.13	δ Sct/SX Phe ^c
V5	189.776219	-40.977123	16.19	0.0724028	20.31	20.12	20.11	0.72	0.37	0.33	δ Sct/SX Phe ^c

Notes.

^a r is the elliptical radius measured from each star to the center of Cen I.

^b Δ_{band} refers to the amplitude of the variable star in a particular band.

^c Milky Way field stars.

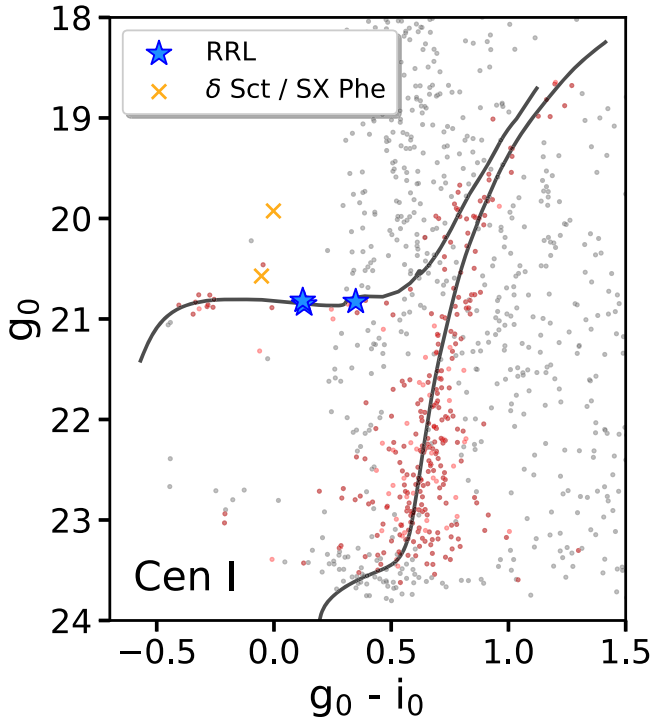


Figure 2. Dereddened CMD of Cen I within $7'$ from the Cen I center (gray points) and its three newly discovered RR Lyrae stars (RRL; blue stars). The black line is the isochrone of 12 Gyr and $Z = 0.0001$ from BaSTI (Hidalgo et al. 2018) shifted to a distance modulus of 20.35 mag (the distance modulus of Cen I obtained in this work, Section 5). The probable members of Cen I ($p_{\text{ugali}} > 0.05$, Mau et al. 2020) are highlighted in red. Orange crosses are the MW field δ Sct/SX Phe stars.

Cen I (red) and MW foreground stars (gray points). The candidate Cen I and MW foreground stars here are selected in a similar manner to those in Pace & Li (2019) and Mau et al. (2020) but updated with Gaia EDR3 astrometry. Briefly, stars are selected based on their location in the CMD, zero parallax, and small proper motions. The remaining stars are used as the input to a proper motion and spatial mixture model to identify the Cen I proper motion and candidate members. More details can be found in Pace & Li (2019) and A. B. Pace et al. (2021, in preparation). The proper motion of CenI-V2 is consistent with the proper motion of Cen I (McConnachie & Venn 2020, A. B. Pace et al. 2021 in preparation). Both δ Sct/SX Phe are consistent with the MW foreground, and the brighter δ Sct/SX Phe, V5, is excluded from being a member of Cen I at high significance based on its proper motion.

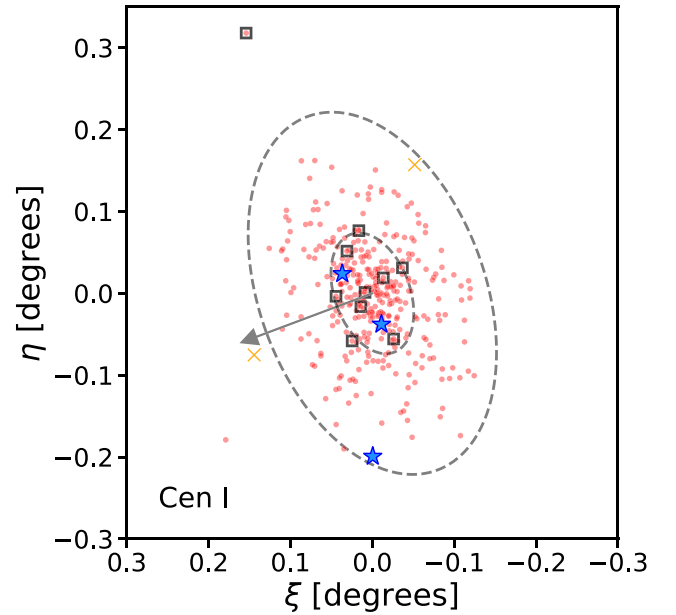


Figure 3. Spatial distribution in planar coordinates for the member candidates of Cen I and the variable stars detected in the field. The three discovered RRL stars in Cen I are shown as blue stars. The members of Cen I are highlighted in red. The 10 blue HB (BHB) members of Cen I are indicated by empty black squares. The ellipses correspond to 2 and 6 r_h ($r_h = 2'3$; Mau et al. 2020). Orange crosses are MW field δ Sct/SX Phe stars. The arrow marks the direction of the reflex-corrected proper motion of Cen I.

Table 3
Gaia EDR3 Proper Motions for the Variable Stars Discovered in the Field of Cen I

Star	Gaia Source_id	$\mu_{\alpha} \cos \delta$ (mas yr ⁻¹)	μ_{δ} (mas yr ⁻¹)
CenI-V1	6146232551449525376
CenI-V2	6146234235076699392	-1.55 ± 1.41	-0.62 ± 1.19
CenI-V3
V4	6146250826534361472	-0.98 ± 1.17	-1.80 ± 0.98
V5	6146230004532587264	-2.31 ± 0.48	-1.11 ± 0.43

5. Distance Determination

RRL stars are considered one of the best standard candles for old stellar systems (Beaton et al. 2018) since they follow a well-known period–luminosity–metallicity (PLZ) relation. In particular, it is in the near-infrared bands where the PLZ relations show the smallest scatter (see, e.g., Cáceres & Catelan 2008;

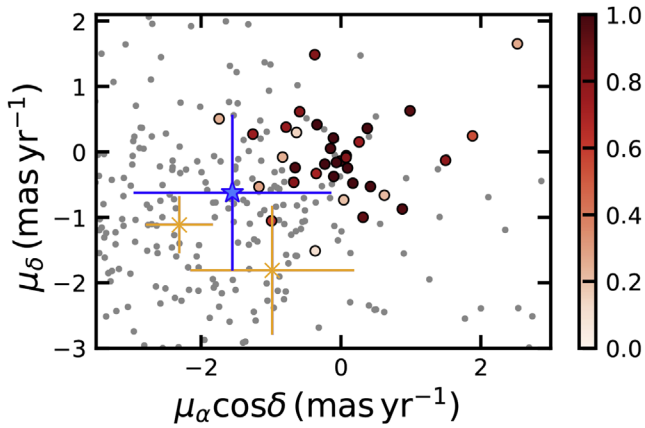


Figure 4. Proper motions from Gaia EDR3 of Cen I field. The gray points represent the proper motions of the field stars nearby (within $30'$) and are consistent with an old, metal-poor isochrone (see Section 4.1 for more details). The reddish dots represent the candidate RGB members. The membership probability is shown in the color bar. The blue star is the proper motion of the RRL star Cen I-V2, and the orange crosses denote the proper motions of the two MW field δ Sct/SX Phe stars.

Marconi et al. 2015; Neeley et al. 2015). Therefore, we use the pulsational properties obtained from the i and z light curves of the RRL stars discovered in this work to derive precise distances.

We employed the PLZ in i and z given by Cáceres & Catelan (2008) to measure the distance moduli to our recently detected RRL stars. The standard uncertainties of these relations are 0.045 mag and 0.037 mag, respectively. For the metallicity, we used the mean metallicity $[\text{Fe}/\text{H}] = -2.57 \pm 0.12$ from Cen I RGB stars obtained from preliminary results of unpublished spectroscopic measurements (J. D. Simon 2021, private communication). For the α abundance, we used $[\alpha/\text{Fe}] = 0.3 \pm 0.2$ based on the average values obtained for other UFD galaxies (e.g., Pritzl et al. 2005; Ji et al. 2019; Simon 2019 and references therein). Therefore, considering the previous values and following the relationship between Z , $[\text{Fe}/\text{H}]$, and $[\alpha/\text{Fe}]$ from Salaris & Cassisi (2005), using $Z_{\odot} = 0.0014$ (Asplund et al. 2021), we obtain $Z = 0.0001$ for Cen I. It is important to note that the Cáceres & Catelan (2008) PLZ relations were obtained in Sloan Digital Sky Survey (SDSS) passbands; therefore, a transformation from SDSS to DES was needed. To do so, we used the following transformation equations that were generated in the same way as the transformation equations obtained by the DES Collaboration using matched stars from DES DR2 and SDSS DR13 in Stripe 82 (DES Collaboration et al. 2021, Appendix A).

$$i_{\text{SDSS}} = i_{\text{DES}} - 0.029 + 0.361(i_{\text{DES}} - z_{\text{DES}}) \quad (1)$$

$$z_{\text{SDSS}} = z_{\text{DES}} - 0.026 + 0.125(i_{\text{DES}} - z_{\text{DES}}). \quad (2)$$

The rms for these relations are 0.016 mag and 0.017 mag, respectively. Also, in order to obtain the true distance modulus (μ_0), we corrected the i - and z -band photometry for dust extinction (see Section 3). The absorption coefficients for the RRL stars of Cen I used in this work can be found in the first two columns of Table 4.

The distance moduli obtained for the RRL stars in Cen I are listed in Table 4. The uncertainties of the individual distance moduli were obtained by propagation of errors considering: (i) the photometric uncertainty of the mean magnitude (0.02 mag), (ii) the dispersion of the filter transformation equation from DES to SDSS (0.02 mag), (iii) the dispersion of the PLZ

(~ 0.04 mag), (iv) the reddening uncertainty (which is usually assumed to be 10%), and (v) the uncertainties of 0.1 dex in $[\text{Fe}/\text{H}]$ and 0.2 dex in $[\alpha/\text{Fe}]$.

For the three RRL stars that are located right on the zero-age HB, which is very well defined because of the high number of blue HBs (BHBs) in this UFD galaxy, we decided not to include the dispersion in magnitude due to evolution since in these cases it seems negligible.

Finally, from the two more confident RRL stars (i.e., Cen I-V1 and Cen I-V2),²⁶ the distance modulus of Cen I $\mu_0 = 20.354 \pm 0.002$ mag ($\sigma = 0.03$ mag), which translates to a heliocentric distance of $D_{\odot} = 117.7 \pm 0.1$ kpc ($\sigma = 1.6$ kpc), with an associated systematic error of 0.07 mag (4 kpc). This value was assessed by fitting simultaneously the RRL stars and comparing the zero-points obtained from the theoretical and semiempirical PLZ relationships in i and z , following the same approach described in Martínez-Vázquez et al. (2015). The inclusion of Cen I-V3 in this analysis would only change the final distance modulus by -0.02 mag.

With the precise distance presented in this work and the Gaia EDR3 proper motions, the addition of spectroscopic radial velocities would complete the 6D phase space information, which can be used to derive an orbit for Cen I.

6. The Oosterhoff Classification of Cen I

Figure 5 shows period versus amplitude (classically known as the Bailey diagram) for the known RRL stars in UFDs with $M_V \gtrsim -6.0$ mag (see Martínez-Vázquez et al. 2019 and Vivas et al. 2020 and references therein). The RRL stars of Cen I are highlighted by blue star symbols.

It is well known that there is a dichotomy between Galactic globular clusters (GGCs) when studying their mean period and their mean metallicity together, the so-called *Oosterhoff dichotomy* (Oosterhoff 1939). There are two types of GGCs (Smith 1995; Catelan 2009; Catelan & Smith 2015, and references therein): *Oosterhoff I* (Oo I) with mean periods for the RRab of ≈ 0.55 days (≈ 0.32 days for the RRc) and mean metallicities between $-1.3 > [\text{Fe}/\text{H}] > -1.7$, and *Oosterhoff II* (Oo II) with mean periods for the RRab of ≈ 0.65 days (≈ 0.37 days for the RRc) and more metal-poor ($[\text{Fe}/\text{H}] < -2.0$) systems.

Figure 5 shows the loci (red curves) provided by Fabrizio et al. (2019) for the RRab stars in Oo I and Oo II type GGCs and that derived by Kunder et al. (2013) for the RRc stars in the cluster M 22, an Oo II GGC. This figure shows how the bulk of RRab stars in UFDs are located around the Oo II line, confirming that UFDs are mainly Oo II systems. Cen I RRL stars seem to overlay well in the Bailey diagram defined by all of the UFD RRL stars. While the two Cen I RRc stars are located near to the Oo II line, the Cen I RRab star is located between Oo I and Oo II lines (i.e., in the Oosterhoff intermediate region). Therefore, due to such a small statistic, it is difficult to make any strong statement about Oosterhoff classification of this galaxy.

Within the context of merger scenarios for the assembly of the Milky Way (Searle & Zinn 1978), the halo formed from the disruption of small galaxies. The properties of the RRL stars in the halo, which are predominantly Oo I (see, e.g., Figure 5 in Drake et al. 2013), do not match those found in the majority of

²⁶ The two RRc stars within $2 r_h$ and complete phase coverage in their light curves.

Table 4
Distance Moduli of the RRL Stars in Cen I

Star	A_i (mag)	A_z (mag)	μ_0 (PLZ _i) (mag)	D_{\odot} (PLZ _i) (kpc)	μ_0 (PLZ _z) (mag)	D_{\odot} (PLZ _z) (kpc)	$\langle\mu_0\rangle$ (mag)	$\langle D_{\odot}\rangle$ (kpc)
Cen I-V1	0.192	0.146	20.38 ± 0.07	119 ± 4	20.33 ± 0.06	116 ± 3	20.35 ± 0.07	117 ± 4
Cen I-V2	0.203	0.155	20.37 ± 0.07	119 ± 4	20.34 ± 0.06	117 ± 3	20.35 ± 0.07	117 ± 4
Cen I-V3	0.177	0.135	20.31 ± 0.07	115 ± 4	20.27 ± 0.06	113 ± 3	20.29 ± 0.07	114 ± 4

Note. The last two columns are the final distance moduli and heliocentric distances for the RRL stars obtained by averaging the PLZ_i and PLZ_z values for each star.

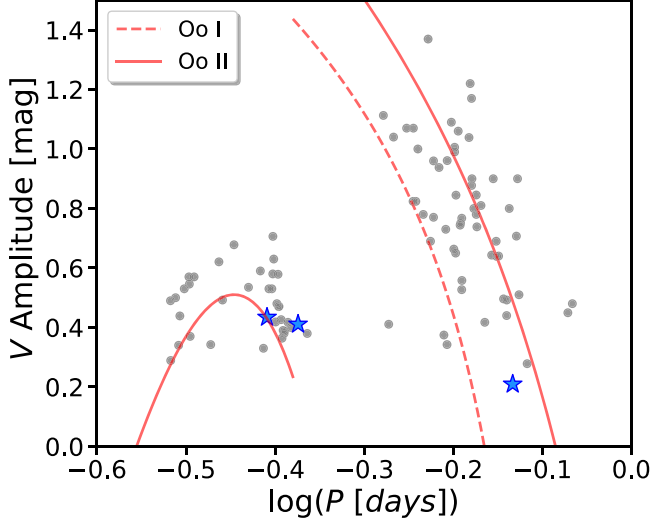


Figure 5. Bailey diagram for the RRL stars found in UFD galaxies with $M_V \gtrsim -6.0$ mag. The RRL stars of Cen I are highlighted with blue stars. The dashed and solid lines are the locus for the RRL stars in Oo I and Oo II Galactic globular clusters (GGCs), respectively.

satellites, except for a few of the more massive and metal-rich systems (Zinn et al. 2014; Fiorentino et al. 2015, 2017). In particular, the fainter dwarf systems (which contain only a few RRL stars) seem to belong preferentially to the Oo II group; therefore, it is clear that UFD galaxies are far from being the main contributors to the Galactic halo (e.g., Vivas et al. 2016, 2020).

7. The Frequency of First Overtone RRL Stars in UFD Galaxies

As can be seen in Figure 2, Cen I hosts a noticeable population of BHB stars. In addition, two of the three RRL stars in Cen I are RRc stars. Theoretical models predict that RRc stars are preferentially located in the blue edge of the instability strip in the HB (e.g., Bono et al. 1995). Since most of the UFDs have a noticeable BHB population, we wanted to investigate in this section if UFDs present a higher ratio of RRc than more massive dwarf galaxies.

In order to check whether there is a higher frequency of RRc stars in UFD galaxies, we study this ratio individually in all of the MW galaxies that have RRL studies so far (see Table 6 in Martínez-Vázquez et al. 2017 for the classical dwarf galaxies and Table A 1 in Martínez-Vázquez et al. 2019 and updates in Vivas et al. 2020 for the UFDs). We note that in this analysis we include RRc and RRd stars due to the fact that some studies are not able to distinguish between them. We refer to them as RRcd stars hereafter.

Figure 6 shows the frequency of RRcd stars, $f_{cd} = N_{RRcd} / (N_{RRab} + N_{RRcd})$, found in MW dwarf galaxies versus their

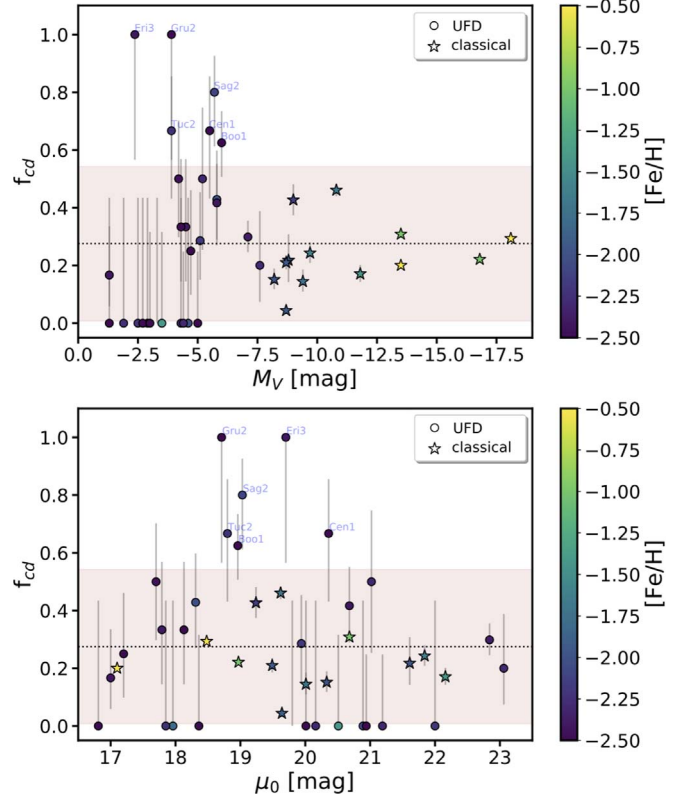


Figure 6. Top: frequency of RRcd stars (f_{cd}) in MW satellite galaxies vs. their absolute magnitude (M_V), color coded by the mean metallicity of the host galaxy. Bottom: same as top panel but as a function of the true distance modulus. The dotted line shows the average of the f_{cd} values. The shaded area represents the 3σ region, and the gray error bars are the Bayesian errors associated with the f_{cd} values. Classical and UFD galaxies are represented by different symbols as shown in the legend.

absolute magnitude (top panel) and their distance moduli (bottom panel). The error bars are the Bayesian errors associated with the f_{cd} values, obtained following Paterno (2004). We color coded the data based on the mean metallicity of the dwarf galaxy. It is clear that there is no particular trend associated with the mass, distance, or metallicity of the host galaxy. The average value of f_{cd} is 0.28 (dashed line), with a dispersion of 0.27 (shaded region). We can see that there are several outliers with $f_{cd} \gtrsim 0.50$: Bootes I, Cen I, Tucana II, Sagittarius II, Grus II, and Eridanus III. All of them are UFD galaxies and have metallicities of $[\text{Fe}/\text{H}] < -2.1$ dex. On the other hand, we see that there are 12 UFD galaxies that do not contain any RRcd stars. However, we can see in Figure 6 that there is no indication that UFD galaxies have a higher ratio of RRcd stars than classical dwarf galaxies and that the outliers ($f_{cd} \gtrsim 0.50$) occur only for UFDs, not for classical dwarfs. In addition, the frequency of RRcd and RRab stars in the UFD

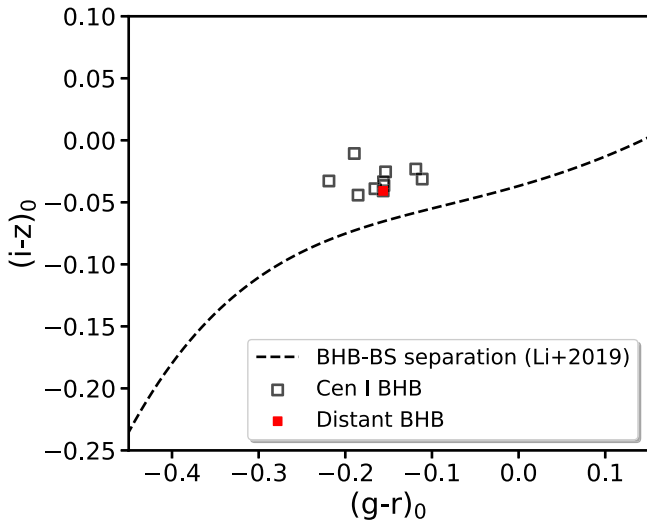


Figure 7. Color-color distribution of BHB stars in Cen I. The dashed curve shows the polynomial in $(g-r)_0$ vs. $(i-z)_0$ proposed by Li et al. (2019) to separate BHB from BS stars.

galaxies is strongly dominated by the small number of RRL stars that belong to them. This is reflected in the dispersion of the f_{cd} , which is 0.31 for the UFDs while for the classical dwarf galaxies is only 0.11. Most of the UFDs that have either a high or null frequency of RRcd stars harbor fewer than five RRL stars. Outliers in f_{cd} are also observed among GGCs (Fabrizio et al. 2021).

On the other hand, if we combine all of the MW UFDs, the mean f_{cd} is 0.29, which is similar to the one obtained for the classical MW dwarfs ($f_{\text{cd}}=0.24$). This indicates that the frequency of RRcd stars is consistent between UFD and classical dwarf galaxies.

8. On the Extension of Cen I

Two of the three discovered RRL stars in Cen I are located within $2 r_h$, at $2'4$ and $3'4$, while the third RRL star (CenI-V3) is at $13'1$ ($\sim 6 r_h$; see Figure 3). In addition, out of the 10 BHB candidates in Cen I, nine are centrally concentrated in the inner $3 r_h$ (see black squares in Figure 3), but the remaining one is located much farther out ($21'4$). In order to check whether these stars are BHB stars at the distance of Cen I or foreground blue straggler (BS) stars, we use our *giz* photometry plus the r photometry from DELVE DR1 and check their positions in the $(g-r)_0$ versus $(i-z)_0$ plane (see Figure 7). Thanks to the BHB-BS separation obtained by Li et al. (2019, their Equation (5)), we see that indeed all of them are in the region of the color-color space where BHB stars are supposed to be (even the BHBs with the largest angular separation).

Both the distant BHB star (located at $21'4$) and the CenI-V3 RRL star (at $13'1$) are located along the major axis of Cen I but in opposite directions, which could be possible evidence of a tidal disruption event (see Figure 3). In the absence of perturbations (e.g., from the LMC), the disruption direction should align with the proper motion vector on the sky. The reflex-corrected proper motion of Cen I (arrow in Figure 3) using the Gaia EDR3 proper motion of Cen I from McConnachie & Venn (2020), the distance from this paper, and positions from Mau et al. (2020) is $(\mu_\alpha \cos \delta, \mu_\delta) = (+0.11, -0.06)$ mas yr $^{-1}$. This is roughly perpendicular to the position angle and would

naively argue against tidal disruption as an explanation for the positions of CenI-V3 and the distant BHB star.

For more insight, we estimated the tidal radius of Cen I. From preliminary analysis of unpublished spectroscopic measurements (J. D. Simon 2021, private communication), the velocity dispersion of Cen I is 5.5 km s^{-1} . For this velocity dispersion, the mass within the half-light radius (using the formula from Wolf et al. 2010) is $2.2 \times 10^6 M_\odot$. Using that mass and the MW potential from Carlin & Sand (2018) in the equation for the Jacobi radius from Binney & Tremaine (2008), the tidal radius of Cen I is 1 kpc (i.e., $29'$). Since this assumed mass for Cen I is very conservative, relying only on the dynamical mass in the central regions of the galaxy, this estimate of the tidal radius can be regarded as a lower limit. Therefore, we conclude that the most distant Cen I RRL star and the most distant BHB star are inside the tidal radius of Cen I. Deeper imaging reaching several magnitudes below the main-sequence turn-off and spectroscopic studies of Cen I will be required to perform a more detailed characterization of its outer regions and possible tidal extension.

9. Conclusions

We present in this work the first study of variable stars in the recently discovered UFD galaxy Cen I. From multi-epoch *giz* DECam observations, we discover three RRL stars in Cen I, and we detect two δ Sct/SX Phe belonging to the MW field.

Two of them are first overtone (RRc) stars, and the remaining one is a fundamental pulsator (RRab) star. The two RRc stars are located within $2 r_h$ while the RRab star (CenI-V3) is at $\sim 6 r_h$. From a smooth distribution of Galactic halo RRL stars, it is not expected to find three MW halo RRL stars clumped together in space at such large distances. In particular, from the density profile of RRL stars derived in Medina et al. (2018), the significance of having three or more MW halo RRL that could contaminate Cen I HB is 4.7σ . Therefore, we conclude that these three RRL stars found are high confidence members of Cen I.

We measure a distance modulus for Cen I of $\mu_0 = 20.354 \pm 0.002$ mag ($\sigma = 0.03$ mag), and a heliocentric distance of $D_\odot = 117.7 \pm 0.1$ kpc ($\sigma = 1.6$ kpc), based on its best sampled RRL stars (i.e., the two RRc stars). The systematic error associated with this measurement due to the uncertainties on the photometry, reddening, $[\text{Fe}/\text{H}]$, and $[\alpha/\text{Fe}]$, is of 0.07 mag (4 kpc). This distance measurement agrees with the distance obtained in the discovery paper by Mau et al. (2020; 20.3 ± 0.1 mag).

The frequency of RRcd stars in MW dwarf galaxies has a mean value of 0.28 with no trend with the M_V , μ_0 , or $[\text{Fe}/\text{H}]$. Some UFDs, including Cen I, present higher RRcd ratios ($f_{\text{cd}} \gtrsim 0.5$), although no strong conclusions can be drawn for individual UFDs due to limited statistics. However, if we combine all of the UFDs, the ratio of RRcd is similar to the one obtained for the classical dwarfs ($f_{\text{cd}} \sim 0.3$). Therefore, the fraction of RRcd stars is consistent between UFD and classical dwarf galaxies.

The location of the Cen I RRL stars in the Bailey diagram is in good agreement with general location of RRL stars from UFD galaxies. Comparing the properties of the RRL stars in UFDs (mainly Oo II) and those from the halo of the MW (mainly Oo I), it is clear that UFDs are far from being the main contributors to the Galactic halo (Vivas et al. 2020). Nevertheless, since UFDs are some of the most ancient systems in the

universe, they can also help us to better understand the hierarchical formation and evolution of our Galaxy.

With the advent of the Vera C. Rubin Legacy Survey of Space and Time (LSST; Ivezić et al. 2019), numerous ultra-faint systems will be discovered. The detection of RRL stars and their role as standard candles is crucial to measuring accurate distances to UFDs. This, in combination with proper motions and spectroscopic data, will allow us to derive their orbits. Thus, time-domain studies of UFDs are necessary to help address questions about their nature, formation, evolution, and contribution to the Galactic halo.

We thank our anonymous referee for the comments and suggestions that have helped to improve the content of this paper.

The DELVE project is partially supported by Fermilab LDRD project L2019-011 and the NASA Fermi Guest Investigator Program Cycle 9 No. 91201.

This work was supported in part by the U.S. Department of Energy, Office of Science, Office of Workforce Development for Teachers and Scientists (WDTS) under the Science Undergraduate Laboratory Internships (SULI) program.

This project used data obtained with the Dark Energy Camera (DECam), which was constructed by the Dark Energy Survey (DES) collaboration. Funding for the DES Projects has been provided by the US Department of Energy, the US National Science Foundation, the Ministry of Science and Education of Spain, the Science and Technology Facilities Council of the United Kingdom, the Higher Education Funding Council for England, the National Center for Supercomputing Applications at the University of Illinois at Urbana-Champaign, the Kavli Institute for Cosmological Physics at the University of Chicago, Center for Cosmology and Astro-Particle Physics at the Ohio State University, the Mitchell Institute for Fundamental Physics and Astronomy at Texas A&M University, Financiadora de Estudos e Projetos, Fundação Carlos Chagas Filho de Amparo à Pesquisa do Estado do Rio de Janeiro, Conselho Nacional de Desenvolvimento Científico e Tecnológico and the Ministério da Ciência, Tecnologia e Inovação, the Deutsche Forschungsgemeinschaft, and the Collaborating Institutions in the Dark Energy Survey.

The Collaborating Institutions are Argonne National Laboratory, the University of California at Santa Cruz, the University of Cambridge, Centro de Investigaciones Energéticas, Medioambientales y Tecnológicas-Madrid, the University of Chicago, University College London, the DES-Brazil Consortium, the University of Edinburgh, the Eidgenössische Technische Hochschule (ETH) Zürich, Fermi National Accelerator Laboratory, the University of Illinois at Urbana-Champaign, the Institut de Ciències de l'Espai (IEEC/CSIC), the Institut de Física d'Altes Energies, Lawrence Berkeley National Laboratory, the Ludwig-Maximilians Universität München and the associated Excellence Cluster Universe, the University of Michigan, NSF's NOIRLab, the University of Nottingham, the Ohio State University, the OzDES Membership Consortium, the University of Pennsylvania, the University of Portsmouth, SLAC National Accelerator Laboratory, Stanford University, the University of Sussex, and Texas A&M University.

Based on observations at Cerro Tololo Inter-American Observatory, NSF's NOIRLab (NOIRLab Prop. ID 2020A-0238; PI: C. E. Martínez-Vázquez), which is managed by the Association of Universities for Research in Astronomy

(AURA) under a cooperative agreement with the National Science Foundation.


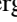


This manuscript has been authored by Fermi Research Alliance, LLC under Contract No. DE-AC02-07CH11359 with the U.S. Department of Energy, Office of Science, Office of High Energy Physics. The United States Government retains and the publisher, by accepting the article for publication, acknowledges that the United States Government retains a nonexclusive, paid-up, irrevocable, world-wide license to publish or reproduce the published form of this manuscript, or allow others to do so, for United States Government purposes.

This work has made use of data from the European Space Agency (ESA) mission Gaia (<https://www.cosmos.esa.int/gaia>), processed by the Gaia Data Processing and Analysis Consortium (DPAC, <https://www.cosmos.esa.int/web/gaia/dpac/consortium>). Funding for the DPAC has been provided by national institutions, in particular the institutions participating in the Gaia Multilateral Agreement.

Facilities: Blanco (DECam), Gaia.

Software: astropy (Astropy Collaboration et al. 2013), matplotlib (Hunter 2007), SExtractor (Bertin & Arnouts 1996).

ORCID iDs

- C. E. Martínez-Vázquez  <https://orcid.org/0000-0002-9144-7726>
 W. Cerny  <https://orcid.org/0000-0003-1697-7062>
 A. K. Vivas  <https://orcid.org/0000-0003-4341-6172>
 A. Drlica-Wagner  <https://orcid.org/0000-0001-8251-933X>
 A. B. Pace  <https://orcid.org/0000-0002-6021-8760>
 J. D. Simon  <https://orcid.org/0000-0002-4733-4994>
 A. R. Walker  <https://orcid.org/0000-0002-7123-8943>
 D. L. Tucker  <https://orcid.org/0000-0001-7211-5729>
 M. Adamów  <https://orcid.org/0000-0002-6904-359X>
 J. L. Carlin  <https://orcid.org/0000-0002-3936-9628>
 Y. Choi  <https://orcid.org/0000-0003-1680-1884>
 P. S. Ferguson  <https://orcid.org/0000-0001-6957-1627>
 A. P. Ji  <https://orcid.org/0000-0002-4863-8842>
 N. Kuropatkin  <https://orcid.org/0000-0003-2511-0946>
 T. S. Li  <https://orcid.org/0000-0002-9110-6163>
 D. Martínez-Delgado  <https://orcid.org/0000-0003-3835-2231>
 S. Mau  <https://orcid.org/0000-0003-3519-4004>
 B. Muflu-Pakdil  <https://orcid.org/0000-0001-9649-4815>
 D. L. Nidever  <https://orcid.org/0000-0002-1793-3689>
 A. H. Riley  <https://orcid.org/0000-0001-5805-5766>
 J. D. Sakowska  <https://orcid.org/0000-0002-1594-1466>
 D. J. Sand  <https://orcid.org/0000-0003-4102-380X>
 G. S. Stringfellow  <https://orcid.org/0000-0003-1479-3059>

References

- Asplund, M., Amarsi, A. M., & Grevesse, N. 2021, *A&A*, 653, A141
 Astropy Collaboration, Robitaille, T. P., Tollerud, E. J., et al. 2013, *A&A*, 558, A33
 Beaton, R. L., Bono, G., Braga, V. F., et al. 2018, *SSRv*, 214, 113
 Bechtol, K., Drlica-Wagner, A., Balbinot, E., et al. 2015, *ApJ*, 807, 50
 Bernstein, G. M., Abbott, T. M. C., Armstrong, R., et al. 2018, *PASP*, 130, 054501
 Bertin, E. 2011, in ASP Conf. Ser., 442, Astronomical Data Analysis Software and Systems XX, ed. I. N. Evans et al. (San Francisco, CA: ASP), 435
 Bertin, E., & Arnouts, S. 1996, *A&AS*, 117, 393
 Binney, J., & Tremaine, S. 2008, in Galactic Dynamics: Second Edition, ed. J. Binney & S. Tremaine (Princeton, NJ: Princeton Univ. Press)

- Bono, G., Caputo, F., & Marconi, M. 1995, *AJ*, **110**, 2365
- Bose, S., Deason, A. J., & Frenk, C. S. 2018, *ApJ*, **863**, 123
- Cáceres, C., & Catelan, M. 2008, *ApJS*, **179**, 242
- Carlin, J. L., & Sand, D. J. 2018, *ApJ*, **865**, 7
- Catelan, M. 2009, *Ap&SS*, **320**, 261
- Catelan, M., & Smith, H. A. 2015, *Pulsating Stars* (New York: Wiley)
- Chambers, K. C., Magnier, E. A., Metcalfe, N., et al. 2016, arXiv:1612.05560
- DES Collaboration, Abbott, T. M. C., Abdalla, F. B., Allam, S., et al. 2018, *ApJS*, **239**, 18
- DES Collaboration, Abbott, T. M. C., Adamow, M., et al. 2021, *ApJS*, **255**, 20
- Drake, A. J., Catelan, M., Djorgovski, S. G., et al. 2013, *ApJ*, **763**, 32
- Drlica-Wagner, A., Bechtol, K., Rykoff, E. S., et al. 2015, *ApJ*, **813**, 109
- Drlica-Wagner, A., Carlin, J. L., Nidever, D. L., et al. 2021, *ApJS*, **256**, 2
- Fabrizio, M., Bono, G., Braga, V. F., et al. 2019, *ApJ*, **882**, 169
- Fabrizio, M., Braga, V. F., Crestani, J., et al. 2021, *ApJ*, **919**, 118
- Fiorentino, G., Bono, G., Monelli, M., et al. 2015, *ApJL*, **798**, L12
- Fiorentino, G., Monelli, M., Stetson, P. B., et al. 2017, *A&A*, **599**, A125
- Flaugher, B., Diehl, H. T., Honscheid, K., et al. 2015, *AJ*, **150**, 150
- Frenk, C. S., & White, S. D. M. 2012, *AnP*, **524**, 507
- Gaia Collaboration, Brown, A. G. A., Vallenari, A., et al. 2021, *A&A*, **649**, A1
- Gaia Collaboration, Brown, A. G. A., Vallenari, A., et al. 2018, *A&A*, **616**, A1
- Gaia Collaboration, Prusti, T., de Bruijne, J. H. J., et al. 2016, *A&A*, **595**, A1
- Hidalgo, S. L., Pietrinferni, A., Cassisi, S., et al. 2018, *ApJ*, **856**, 125
- Holl, B., Audard, M., Nienartowicz, K., et al. 2018, *A&A*, **618**, A30
- Horne, J. H., & Baliunas, S. L. 1986, *ApJ*, **302**, 757
- Hunter, J. D. 2007, *CSE*, **9**, 90
- Ivezić, Ž., Kahn, S. M., Tyson, J. A., et al. 2019, *ApJ*, **873**, 111
- Ji, A. P., Simon, J. D., Frebel, A., Venn, K. A., & Hansen, T. T. 2019, *ApJ*, **870**, 83
- Kunder, A., Stetson, P. B., Cassisi, S., et al. 2013, *AJ*, **146**, 119
- Layden, A. C. 1998, *AJ*, **115**, 193
- Li, T. S., Koposov, S. E., Zucker, D. B., et al. 2019, *MNRAS*, **490**, 3508
- Marconi, M., Coppola, G., Bono, G., et al. 2015, *ApJ*, **808**, 50
- Martínez-Vázquez, C. E., Monelli, M., Bernard, E. J., et al. 2017, *ApJ*, **850**, 137
- Martínez-Vázquez, C. E., Monelli, M., Bono, G., et al. 2015, *MNRAS*, **454**, 1509
- Martínez-Vázquez, C. E., Salinas, R., & Vivas, A. K. 2021, *AJ*, **161**, 120
- Martínez-Vázquez, C. E., Stetson, P. B., Monelli, M., et al. 2016, *MNRAS*, **462**, 4349
- Martínez-Vázquez, C. E., Vivas, A. K., Gurevich, M., et al. 2019, *MNRAS*, **490**, 2183
- Mau, S., Cerny, W., Pace, A. B., et al. 2020, *ApJ*, **890**, 136
- McConnachie, A. W., & Venn, K. A. 2020, *RNAAS*, **4**, 229
- Medina, G. E., Muñoz, R. R., Vivas, A. K., et al. 2018, *ApJ*, **855**, 43
- Morganson, E., Gruendl, R. A., Menanteau, F., et al. 2018, *PASP*, **130**, 074501
- Neeley, J. R., Marengo, M., Bono, G., et al. 2015, *ApJ*, **808**, 11
- Oosterhoff, P. T. 1939, *Obs*, **62**, 104
- Oosterhoff, P. T. 1944, *BAN*, **10**, 55
- Pace, A. B., & Li, T. S. 2019, *ApJ*, **875**, 77
- Paterno, M. 2004, Calculating efficiencies and their uncertainties, Technical Report, *FERMILAB-TM-2286-CD*
- Pritzl, B. J., Venn, K. A., & Irwin, M. 2005, *AJ*, **130**, 2140
- Salaris, M., & Cassisi, S. 2005, *Evolution of Stars and Stellar Populations* (New York: Wiley)
- Savino, A., Koch, A., Prudil, Z., Kunder, A., & Smolec, R. 2020, *A&A*, **641**, A96
- Schlafly, E. F., & Finkbeiner, D. P. 2011, *ApJ*, **737**, 103
- Schlegel, D. J., Finkbeiner, D. P., & Davis, M. 1998, *ApJ*, **500**, 525
- Searle, L., & Zinn, R. 1978, *ApJ*, **225**, 357
- Simon, J. D. 2019, *ARA&A*, **57**, 375
- Smith, H. A. 1995, *RR Lyrae Stars*, Cambridge Astrophysics Series, Vol. 27 (Cambridge: Cambridge Univ. Press), 27
- Sokolovsky, K. V., Gavras, P., Karamelas, A., et al. 2016, *MNRAS*, **464**, 274
- Stetson, P. B., Fiorentino, G., Bono, G., et al. 2014, *PASP*, **126**, 616
- Tolstoy, E., Hill, V., & Tosi, M. 2009, *ARA&A*, **47**, 371
- Tonry, J. L., Denneau, L., Flewelling, H., et al. 2018, *ApJ*, **867**, 105
- Vivas, A. K., Alonso-García, J., Mateo, M., Walker, A., & Howard, B. 2019, *AJ*, **157**, 35
- Vivas, A. K., Martínez-Vázquez, C., & Walker, A. R. 2020, *ApJS*, **247**, 35
- Vivas, A. K., Olsen, K., Blum, R., et al. 2016, *AJ*, **151**, 118
- Walker, A. R. 1989, *PASP*, **101**, 570
- White, S. D. M., & Frenk, C. S. 1991, *ApJ*, **379**, 52
- Willman, B., Blanton, M. R., West, A. A., et al. 2005a, *AJ*, **129**, 2692
- Willman, B., Dalcanton, J. J., Martinez-Delgado, D., et al. 2005b, *ApJL*, **626**, L85
- Wolf, C., Onken, C. A., Luvaul, L. C., et al. 2018, *PASA*, **35**, e010
- Wolf, J., Martinez, G. D., Bullock, J. S., et al. 2010, *MNRAS*, **406**, 1220
- Zinn, R., Horowitz, B., Vivas, A. K., et al. 2014, *ApJ*, **781**, 22